



JOINT INSTITUTE FOR NUCLEAR RESEARCH
Frank laboratory of Neutron Physics

FINAL REPORT ON THE START PROGRAMME

*Influence of proton and gamma radiation on
the properties of n-type and p-type silicon
structures*

Supervisor:

Dr. Aleksandr Sergeevich
Doroshkevich

Student:

Dilmurod Rakhmanov,
Uzbekistan
Institute of Semiconductor
physics and microelectronics
at the NUUz

Participation period:

July 17 – August 27, 2022

Dubna, 2022

Contents

1.Abstract.....	3
2.Introduction.....	4
3.Methods.....	6
4.Results.....	16
4.Conclusion.....	25
5.Acknowledhments.....	25
6.References.....	26

Abstract

In this work, the effect of implanted hydrogen ions on the properties of silicon samples doped with transition elements was studied. For the study, single-crystal silicon samples of n-type and p-type were used, which were doped with phosphorus and boron during rotation. These samples were irradiated with protons with an energy of 2 MeV and a current of 0.5 μA at an irradiation dose of $5.6 \times 10^{14} \text{ cm}^{-2}$ at room temperature (300⁰ K). To study the properties of silicon samples before and after irradiation, impedance methods were used to determine the electrical properties of the samples, Raman spectroscopy to determine the composition of silicon, IR spectroscopy to determine the concentration of optical active oxygen, Ellipsometry to determine the optical properties and layers that were created after doping and irradiation, volt-ampere characteristics.

Introduction

The relevance of the study. In recent years, all over the world in the field of rapidly developing semiconductor micro-, opto- and nanoelectronics, one of the promising areas is the development of ways of the physical modification of single-crystal silicon. In this regard, studies aimed at studying the effect of various types of radiation on the electrical properties of silicon doped with transition element impurities and establishing controlled methods for improving the thermal stability and radiation resistance of the parameters of silicon devices are one of the important problems.

According to the available literature data the most important scientific tasks today are:

1.) - the study of the processes of formation of radiation defect centers in Si after irradiation doped with impurities of transition elements;
2.) - the effect of various types of radiation on the electrophysical properties of silicon with impurities of transition elements;
3.) - influence of thermal and radiation defects on the formation of a defect structure of Si with impurities of transition elements;
4.) - identification of the energy spectrum of deep levels created by impurities of transition elements;
5.) - interactions of specially introduced impurities with structural lattice defects.

This work is devoted to solving these problems using spectral analytical methods.

The degree of knowledge of the problem. Analysis and generalization of the results of research conducted by well-known experts in the field of semiconductor physics and semiconductor nano- and microelectronics (V.A. Kozlov, V.V. Kozlovsky, V.V. Petrov, G.S. Kulikov, A.A. Lebedev, Weber, W.Wondrak, D.Silber and others) show that experimental studies of optical, electrophysical, resonant and other properties of semiconductors irradiated with various radiations,

among which PE impurities in Si occupy a special place, today make it possible to build certain general models of radiation deep centers, but these models are not yet perfect.

Despite the large number of experimental data on the study of the electrophysical properties of irradiated semiconductors and semiconductor structures, there is still no picture that makes it possible to predict the behavior of silicon and structures based on it under irradiation with protons.

The aim of the study is to study the change in the electrical properties of Si doped with impurities of transition elements - platinum, chromium and radiation defect formation after irradiation with protons.

To achieve this goal, it was necessary to solve the following tasks:

To investigate the electrophysical properties of Si samples doped with transition elements - Pt and Cr as a diffusion way;

Irradiate Si samples doped with transition elements with protons;

Measure the electrophysical properties of Si samples doped with transition elements and irradiated samples;

Compare electrophysical properties of Si samples doped with transition elements and irradiated samples with protons;

The object of study is single-crystal silicon grown by the Czochralski method, as well as Si doped with platinum and chromium.

Research methods. For research, the methods of impedance spectroscopy, Raman spectroscopy, current-voltage characteristic and infrared (IR) absorption were used. An electrostatic accelerator EG-5 for irradiation of samples were used.

Practical significance of the research results. The results obtained can be used in the development of radiation-resistant semiconductor devices.

2. Methods

1. Electrophysical property measurement technique Impedance spectroscopy

Electrochemical impedance spectroscopy (EIS): EIS is one of the most informative electrochemical techniques.

In a conventional electrochemical cell a medium–electrode interactions includes the concentration of electroactive elements, charge-transfer, and mass-transfer (diffusion) from the bulk solution to the electrode surface in addition to the resistance of the electrolyte. Each of these features is characterized by an electrical circuit that consists of resistances, capacitors, or constant phase elements that are connected in parallel or in a series to form an equivalent circuit, as shown¹ in Figure 1. Thus, the EIS could be used to explore mass-transfer, charge-transfer, and diffusion processes. Accordingly, the EIS has the ability to study intrinsic material properties or specific processes that could influence conductance, resistance, or capacitance of an electrochemical system. The impedance differs from the resistance, since the resistance observed in DC circuits obeys Ohm’s Law directly. A small signal excitation is applied for measuring the impedance response. The electrochemical cell response is pseudo-linear in which a phase-shift is acquired while the current response to a sinusoidal potential is a sinusoid at the applied frequency. Thus, the excitation signal is presented as a function of time, as shown in Equation (1):

$$E_t = E_0 \cdot \sin(\omega t) \quad (1)$$

where E_t is the potential at time t , E_0 is the amplitude of the signal, and ω is the radial frequency.

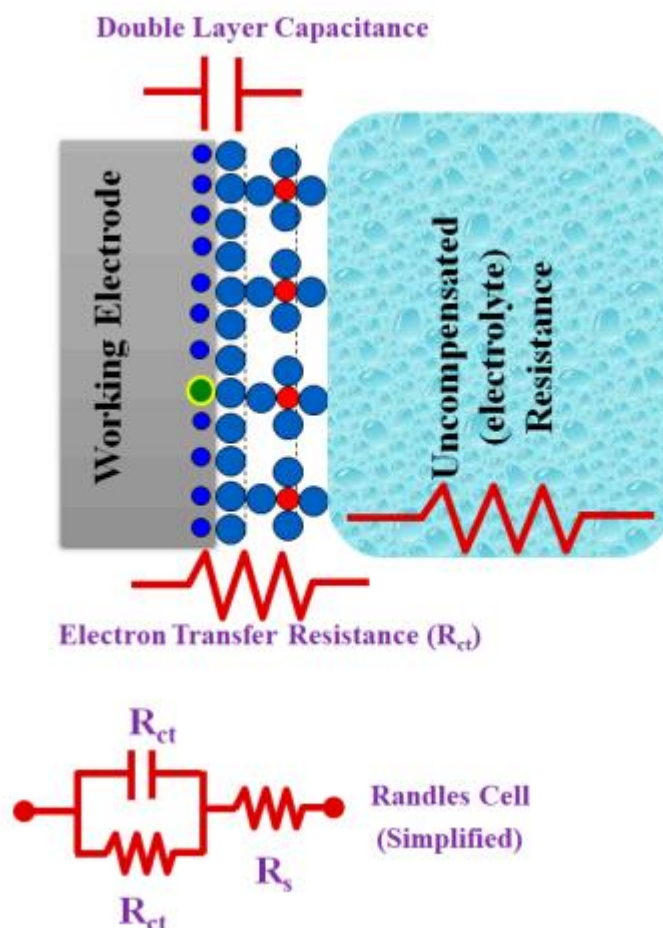


Figure 1. A simple scheme to describe the EIS circuit and the redox reaction takes place at the surface of working electrodes in a conventional-electrochemical cell (i.e., three-electrode system). R_{ct} is the charge transfer resistance, R_s is electrolyte resistance, and C_{dl} is the capacitance double layer.

The correlation between the radial frequency (ω) and the applied frequency (f) is calculated by Equation (2):

$$\omega = 2 \cdot \pi \cdot f \quad (2)$$

In a linear system, the signal is shifted in phase (Φ) and has a different amplitude than I_0 (Equation (3)):

$$I_t = I_0 \sin(\omega t + \Phi) \quad (3)$$

Thus, the impedance of the whole system can be obtained from Equation (4):

$$Z = E/I = Z_0 \exp(i\Phi) = Z_0 (\cos\Phi + i\sin\Phi) \quad (4)$$

Where: Z , E , I , ω , and Φ are impedance, potential, current, frequency, and phase shift between E and I , respectively. The impedance is expressed in terms of a magnitude, Z_0 , and a phase shift, Φ . If the applied sinusoidal signal is plotted on the X-axis and the sinusoidal response signal (I) on the Y-axis, the result is a “Lissajous Plot”, Figure 2(I). Before the existence of modern EIS instrumentation, Lissajous analysis was the only way for the impedance measurement^{2,3}.

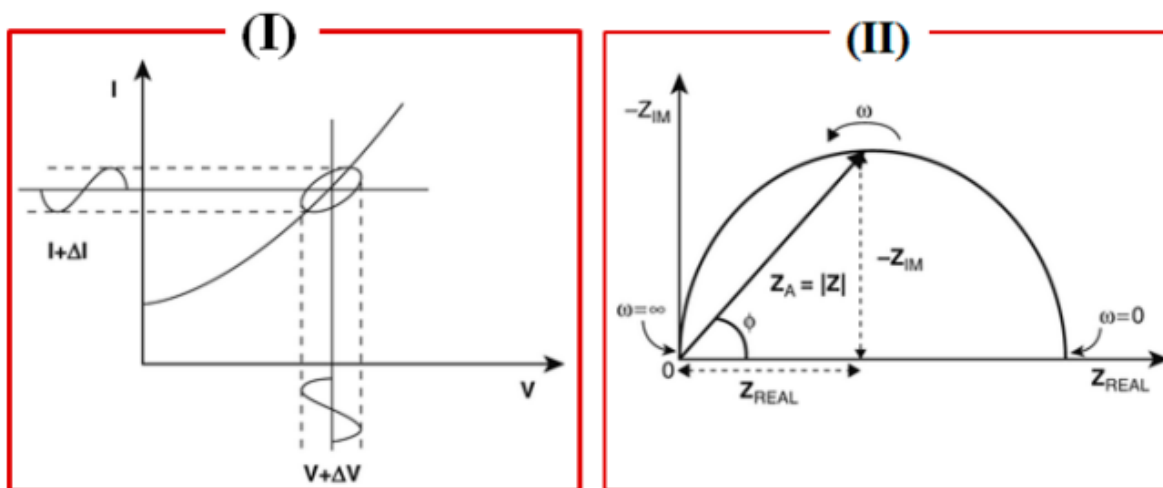


Figure 2. The Lissajous plot (I) and Nyquist plot with impedance vector (II)

Electrochemical processes associated with the electrolyte/interface and redox reactions are simulated/computed as an electric circuit (equivalent circuit) involving electrical components (resistors, capacitors, inductors). This equivalent circuit is designed and implemented to understand and evaluate the individual components of the EIS system. Resistance of solution (R_s), double layer capacitance at the surface of the electrode (C_{dl}), charge transfer resistance (R_{ct}), and Warburg resistance (Z_w) are simplified in the Randles equivalent circuits, as shown⁴ in Figure 3. Warburg resistance is the result of a diffusion process occurring at the electrode–electrolyte interface. Experimentally, the perfect capacitor does not regularly exist, thus an additional element called a constant phase element (CPE) is applied to mimic/model this non-ideal capacitance behavior. The discussed reasons behind this include surface roughness, non-homogeneity, or surface porosity of the investigated materials⁵.

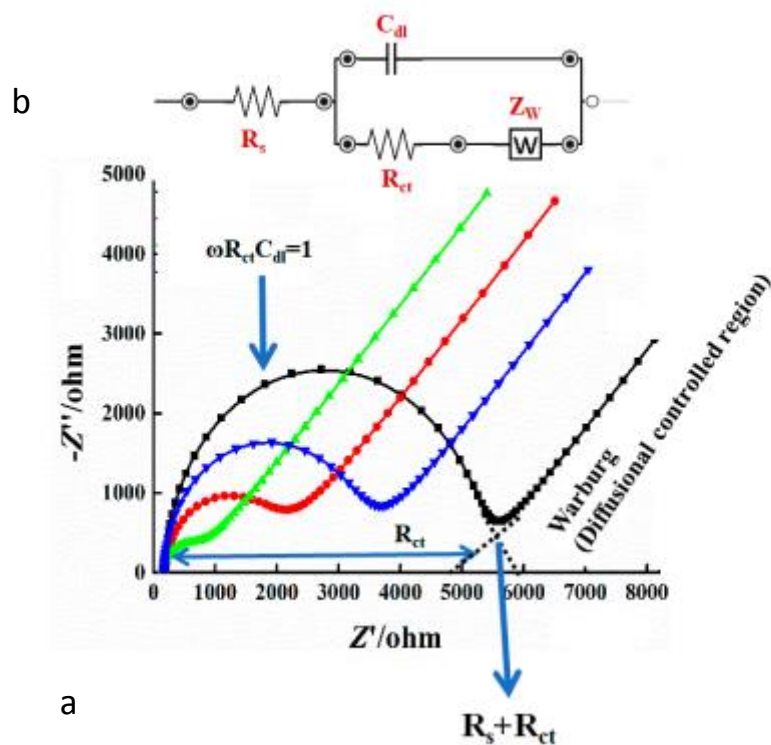


Figure 3. Impedance spectras showing a simplified Randles (a) equivalent circuit (b) for an electrochemical system (original data obtained by our team).

From Nyquist plots (practical data must be obtained first), elements of the equivalent circuit are determined and connected according to the Nyquist shape. Therefore, the EIS curve is the most important datum to be obtained first, and then surface characteristics are evaluated from fitting the electrical circuit simulation (see Figure 4). The shape of a Nyquist plot is dependent on the electrode matrix (i.e., working electrode composition) and the electrochemical responses taking place either at the surface of the working electrode or in the bulk solution. Thus, different Nyquist plot curves could be generated, e.g., a single semicircle, two semicircles, or two half-semicircles could be obtained for specific electrochemical operation⁶.

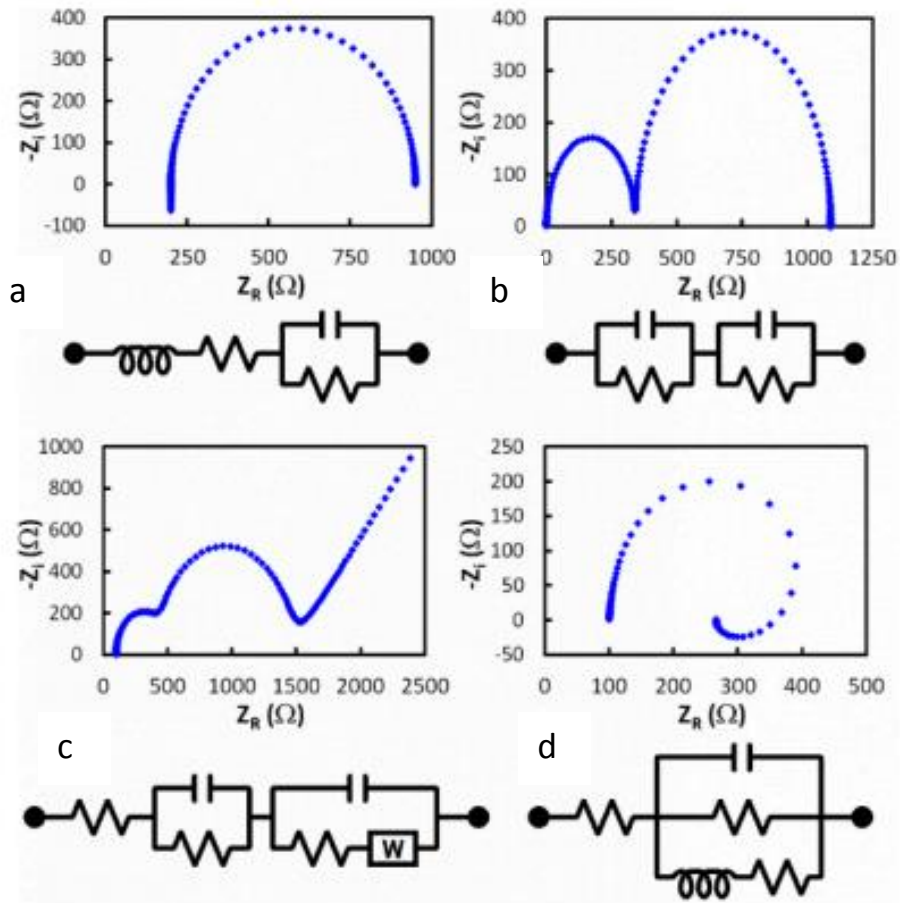


Figure 4. Impedance spectra (examples of Nyquist plot curves) of single-phase samples (a), two-phase samples (b), three-phase samples (c) and a samples with the effect of negative capacitance (d) and their equivalent circuits).

Physical and chemical processes in fuel cells as well as energy storage devices can be characterized effectively using the EIS technique as a non-destructive investigating tool. Thus, the EIS can be implemented to monitor stability and performance of these materials and devices in addition to monitoring their charge transport-properties⁷.

2.2. Spectra measurement technique Raman spectroscopy

Raman spectroscopy is a non-destructive analysis technique that provides detailed information about chemical bonds, crystal phase and molecular interactions. It is based on the interaction of light with electronic subsystem of materials⁸.

The Raman spectrum has a number of peaks indicating the intensity and position of the wavelength of the Raman scattered light. Each peak corresponds to a specific molecular bond vibration, including individual bonds such as C-C, C=C, NO, C-H, etc., and bond groups such as benzene ring breathing mode, polymer chain vibrations, lattice modes, etc.

Raman spectroscopy investigates the chemical structure of a material and provides information about¹⁰:

- Chemical composition and stoichiometry of the substance
- Phase and polymorphism
- Internal stress/deformation
- Pollution and impurities

Typically, a Raman spectrum is a distinct chemical fingerprint for a particular molecule or material, and can be used to very quickly identify a material or distinguish it from others. Raman spectra libraries are often used to identify a material based on its Raman spectrum—libraries containing thousands of spectra are quickly scanned to find a match with the spectrum of the analyte¹¹.

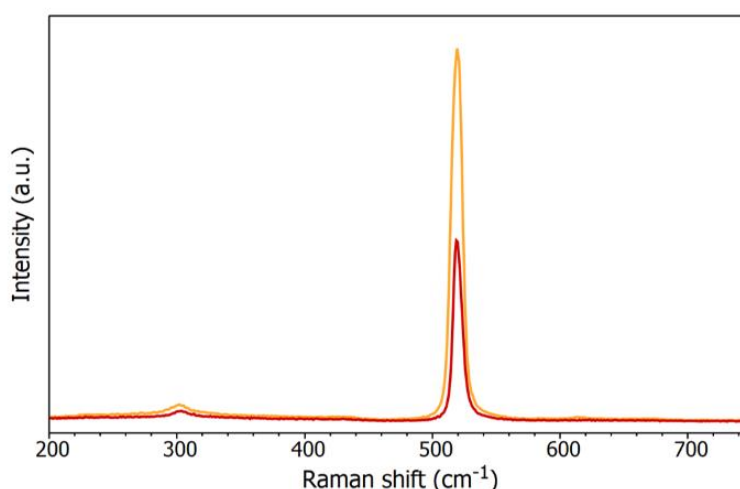


Fig.5. Raman spectrum of initial silicon.

The overall spectrum profile (peak position and relative peak intensity) provides a unique chemical fingerprint that can be used to identify a material and distinguish it from others. Often the actual spectrum is quite complex, so extensive libraries of Raman spectra can be searched to find a match and thus provide chemical identification.

The intensity of the spectrum is directly proportional to the concentration. Typically, a calibration procedure will be used to determine the relationship between peak intensity and concentration, and then routine measurements can be performed to analyze the concentration. For mixtures, relative peak intensities provide information on the relative concentration of the components, while absolute peak intensities can be used to provide information on absolute concentrations¹².

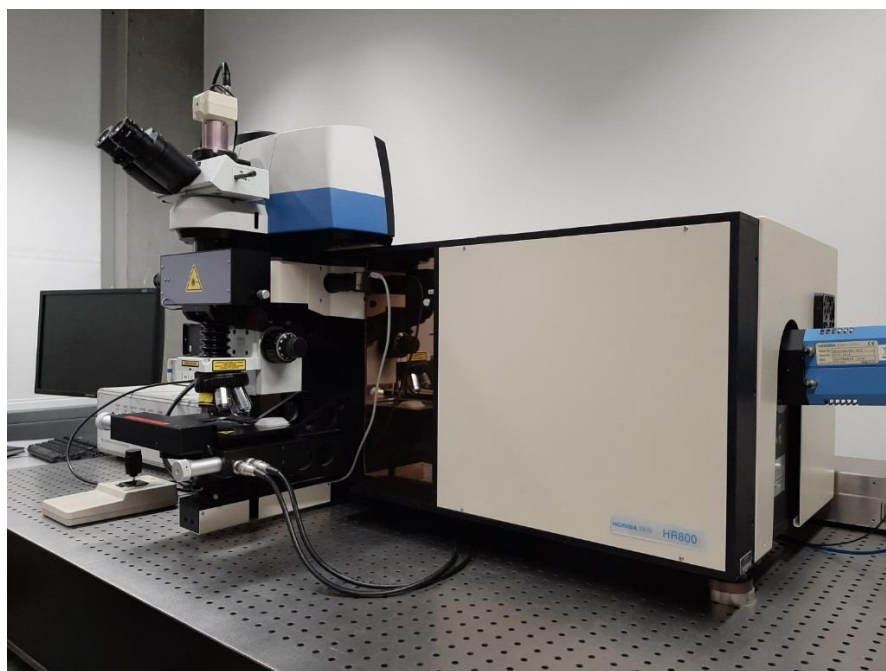


Fig.6. Confocal Raman microscope SENTERRA II with laser safety case.

Raman spectroscopy can be used for microscopic analysis with a spatial resolution on the order of 0.5–1 μm . Such an analysis is possible using a Raman microscope.

A Raman microscope connects a Raman spectrometer to a standard optical microscope, allowing high magnification imaging of the sample and Raman analysis with a microscopic laser spot¹³.

A true confocal Raman microscope can be used to analyze particles or micron-sized volumes. It can even be used to analyze different layers in a multilayer sample (eg polymer coatings) as well as contaminants and features below the surface of a transparent sample (eg impurities in glass and liquid/gas inclusions in minerals).

Motorized mapping steps generate Raman spectral images that contain many thousands of Raman spectra obtained from different positions on the sample¹⁴. The Raman spectrum can be used to create false color images that show the distribution of individual chemical components and changing other effects such as phase, polymorphism, stress/strain, and crystallinity.

2.3 IR-Spectroscopy

Infrared spectroscopy is based on the measurement of the interaction of infrared radiation with matter by absorption, emission, or reflection. It is used to study and identify chemical substances or functional groups in solid, liquid, or gaseous forms. It can be used to characterize new materials or identify and verify known and unknown samples. The method or technique of infrared spectroscopy is conducted with an instrument called an infrared spectrometer (or spectrophotometer) which produces an infrared spectrum. An IR spectrum can be visualized in a graph of infrared light absorbance (or transmittance) on the vertical axis vs. frequency, wavenumber or wavelength on the horizontal axis. Typical units of wavenumber used in IR spectra are reciprocal centimeters, with the symbol cm^{-1} . Units of IR wavelength are commonly given in micrometers (formerly called "microns"), symbol μm , which are related to the wavenumber in a reciprocal way. A common laboratory instrument that uses this technique is a Fourier transform infrared (FTIR) spectrometer.

The infrared portion of the electromagnetic spectrum is usually divided into three regions; the near-, mid- and far- infrared, named for their relation to the visible spectrum. The higher-energy near-IR, approximately $14,000\text{--}4,000\text{ cm}^{-1}$ ($0.7\text{--}2.5\text{ }\mu\text{m}$ wavelength) can excite overtone or combination modes of molecular vibrations. The mid-infrared, approximately $4,000\text{--}400\text{ cm}^{-1}$ ($2.5\text{--}25\text{ }\mu\text{m}$) is generally used to study the fundamental vibrations and associated rotational-vibrational structure. The far-infrared, approximately $400\text{--}10\text{ cm}^{-1}$ ($25\text{--}1,000\text{ }\mu\text{m}$) has low energy and may be used for rotational spectroscopy and low frequency vibrations. The region from $2\text{--}130\text{ cm}^{-1}$, bordering the microwave region, is considered the terahertz region and may probe intermolecular vibrations.^[1] The names and classifications of these subregions are conventions, and are only loosely based on the relative molecular or electromagnetic properties.

Infrared spectroscopy exploits the fact that molecules absorb frequencies that are characteristic of their structure. These absorptions occur at resonant frequencies, i.e. the frequency of the absorbed radiation matches the vibrational frequency .

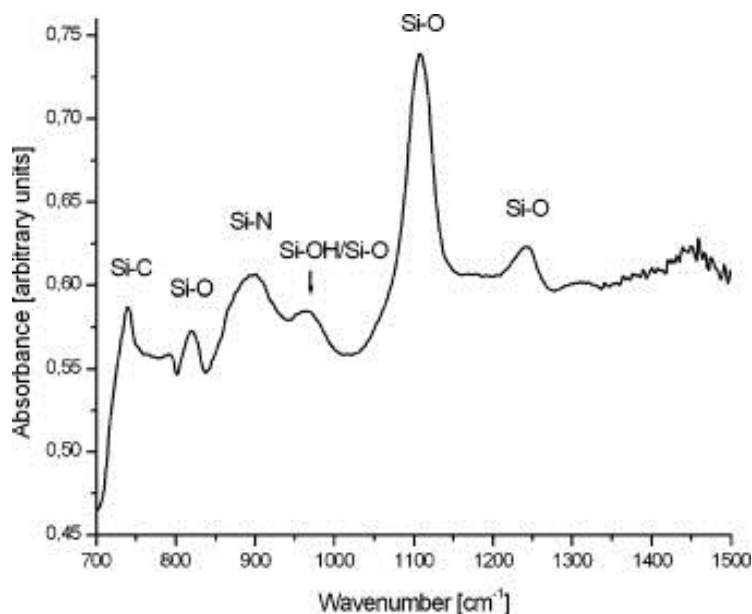


Figure.7.IR-spectrum of Silicon monocrystalline.

In particular, in the Born–Oppenheimer and harmonic approximations, i.e. when the molecular Hamiltonian corresponding to the electronic ground state can be

approximated by a harmonic oscillator in the neighborhood of the equilibrium molecular geometry, the resonant frequencies are associated with the normal modes of vibration corresponding to the molecular electronic ground state potential energy surface.

The resonant frequencies are also related to the strength of the bond and the mass of the atoms at either end of it. Thus, the frequency of the vibrations are associated with a particular normal mode of motion and a particular bond type.

The infrared spectrum of a sample is recorded by passing a beam of infrared light through the sample. When the frequency of the IR is the same as the vibrational frequency of a bond or collection of bonds, absorption occurs. Examination of the transmitted light reveals how much energy was absorbed at each frequency (or wavelength). This measurement can be achieved by scanning the wavelength range using a monochromator. Alternatively, the entire wavelength range is measured using a Fourier transform instrument and then a transmittance or absorbance spectrum is generated using a dedicated procedure¹⁶.

3 Results

3.1. Electrical properties of semiconductor heterostructures based on silicon KEF-0.3 after irradiation with gamma quantum

The high sensitivity of single-crystal silicon and silicon devices to the effects of radiation has led to the fact that recently the problems of the effect of radiation on the electrophysical properties of materials, characteristics, reliability and stability of space semiconductor electronics devices have become very relevant.

It is known that in semiconductor materials used for the manufacture of solar cells, including single-crystal silicon, the concentration, mobility, and lifetime of charge carriers change during the action of penetrating radiation, due to the appearance of radiation defects¹⁷.

For the experiments we used n-type silicon grown by the Czochralski method with a resistivity of 0.3 $\Omega \cdot \text{cm}$ (KEF-0.3). The initial silicon was doped with phosphorus (n-Si) during growth and the dopant concentration was $7.3 \times 10^{13} \div 7.1 \times 10^{15} \text{ cm}^{-3}$. Irradiation of silicon samples with γ -quanta was carried out in stages: $\Phi = 10^5, 10^6, 10^7, 10^8$ rad using the isotope Co_{60} (1.17 MeV) at a temperature $T_{\text{rad}} = 300 \text{ K}$.

To obtain the current-voltage characteristics of the samples, a P-20 potentiostat (Elins) was used. Determined the value of the current in the voltage range from -5 to 10 volts.

Figure 8 shows the current–voltage characteristics of the original (curve 1) and irradiated samples (curves 2–5 (1–4 in the inset of Fig. 8, b)). There is a sharp drop in electrical conductivity and rectifying properties. All irradiated samples showed an almost 10-fold decrease in the maximum current on the forward branch (60 to 10 mA at 10 V), and more than 5-6 times (from 10 to 2 mA at -5 V) on the reverse branch of the V-I characteristics.

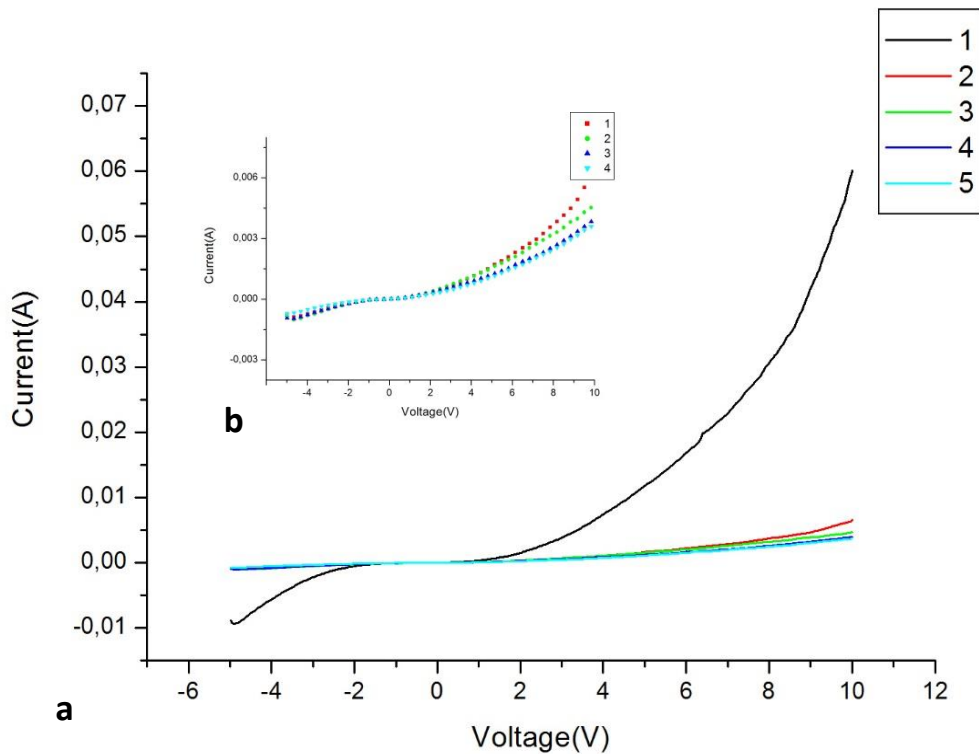


Fig.8. Current-voltage characteristics of silicon samples before (curve 1) and after irradiation with doses of 10^5 rad (curve 2), 10^6 rad (curve 3), 10^7 rad (curve 4) and 10^8 rad (curve 5), respectively (Fig. 8, a).

Inset (Fig. 1b) Current-voltage characteristics of irradiated samples with doses of 10^5 rad (curve 1), 10^6 rad (curve 2), 10^7 rad (curve 3), and 10^8 rad (curve 4), respectively.

The difference in the maximum current for all irradiated samples was about 0.001-0.002 A (depending on the radiation dose).

The results obtained correlate with the results of article¹⁸, according to which irradiation of any nature leads to a decrease in the electrical conductivity of semiconductors.

The most significant factor in changing the properties of irradiated silicon are radiation defects containing V vacancies. Such radiation defects include the O_i -V interstitial oxygen complex (A-center), doublet vacancy (V-V), and the phosphorus complex at the P_s -V vacancy site (E-center). All these radiation defects are effective recombination centers, and traps of free charge carriers responsible for their accumulation in the crystal and the subsequent increase in the resistivity of irradiated silicon¹⁹.

A proportional dependence of the specific resistance of the silicon structure under study on the value of the imparted dose has been established.

3.2. Effect of proton irradiation on the oxygen content of n-Si silicon samples

Currently, the use of alternative energy sources is one of the most important issues in various fields. The basis of alternative energy sources is occupied by solar photocells. At a time when the use of solar cells is expanding, there are a problems of studying the physical factors affecting their performance and efficiency. In particular, there is a negative effect of temperature and radiation on the efficiency of solar cells when it's uses on space stations, and in dusty areas with high levels of environmental pollution²⁰.

Silicon monocrystals are mainly used in the production of solar photovoltaic cells. The study and elimination of external adverse effects on silicon solar cells is one of the urgent tasks in the energy sector.

The purpose of this work was to study the effect of proton irradiation on the oxygen content of n-Si silicon samples using IR spectroscopy.

For the experiments we used n-type silicon grown by the Czochralski method with a resistivity of 40 Ω cm (KEF-40). The initial silicon was doped with phosphorus (n-Si) during growth and the dopant concentration was $5 \times 10^{13} \div 5.3 \times 10^{15}$ cm^{-3} . Irradiation of silicon samples with hydrogen ions was carried out in an electrostatic accelerator "EG-5" with an energy of 2 MeV, a current of 0.5 μA and a dose of 5.1×10^{14} cm^{-2} at a temperature of $T = 300$ K.

To determine the concentration of optical active oxygen in silicon samples, an IR spectrometer "Shimadzu IRAffinity-1" was used. The measurement was carried out in the range of 400 - 2000 cm^{-1} wavenumber.

It is known²¹ that oxygen can be present in single-crystal silicon in various forms (in an atomically dispersed state and in the form of various complexes). In the dispersed state, oxygen is in the interstitial position, forming with two neighboring

silicon atoms a quasi-molecule Si - O - Si. In this case, the oxygen atoms that are part of the Si - O - Si quasimolecule are optically active and have a number of natural vibrational frequencies of 1225, 1106, 515 cm^{-1} (at $T = 300 \text{ K}$). As the temperature decreases, these bands shift, split, and change in intensity. The most intense IR absorption band is the band at 1106 cm^{-1} (9.1 μm), and therefore, in practice, this band is used to determine the atomic oxygen content in the crystal. It turns out that the concentration of optical active oxygen ($N_{\text{O}}^{\text{opt}}$) is proportional to the absorption coefficient α_{max} at the maximum of the 1106 cm^{-1} band²²:

$$N_{\text{O}}^{\text{opt}} = K \cdot \alpha_{\text{max}}(1106 \text{ cm}^{-1}) \quad (1)$$

Where K is the coefficient of proportionality.

Figure 9 shows the IR spectra of the original (black line) and irradiated (red line) n-type silicon samples. We can see that the IR spectra show us several peaks, but of these, we are only interested in one peak that was created with a high intensity in the wavenumber of 1106 cm^{-1} . This peak belongs to optically active oxygen, which is in the interstitial position, forming a Si-O-Si quasi-molecule with two neighboring silicon atoms.

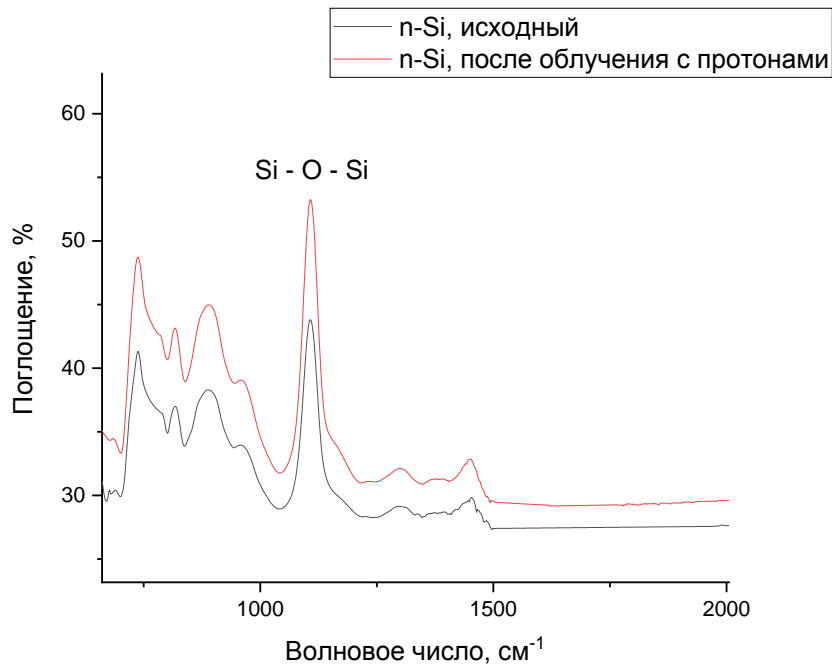


Fig.9. IR spectra of initial and irradiated n-Si silicon samples.

A comparison of the IR absorption spectra of the original and irradiated samples show that the introduction of hydrogen ions into silicon after irradiation leads to a significant increase (about 10–15%) in the concentration of optically active oxygen.

Analysis of the obtained results leads to the following conclusions. Irradiation of silicon samples leads to the release of oxygen atoms located in the crystal lattice sites associated with silicon atoms, and one of the famous radiation defects, A-centers (V-O), is formed. It also causes the oxygen atoms at the outer site to move between sites. As a result, we see that irradiation increases the concentration of optically active oxygen.

3.3. Study of the influence of proton irradiation on silicon structures using Raman spectroscopy

Modification of semiconductor materials, directed change of their properties, by beams of light ions, in particular protons, is one of the most promising and rapidly developing physical and technological methods in recent years. Interest in protons is due to the wide and controllable range of processed material depths (from 0.1 μm to 1 mm) and the absence of complex radiation complexes with a high annealing temperature after proton irradiation. The main three factors influencing the change in the properties of semiconductors after proton irradiation are: a change in the electrophysical properties of semiconductors, radiation defect formation, and the accumulation of hydrogen atoms²⁴.

To study the effect of proton irradiation on silicon, we used Raman spectroscopy.

Lasers on such working bodies as Ar + (351.1-514.5 nm), Kr + (337.4-676.4 nm), and He-Ne (632.8 nm) are mainly used as a source of exciting light²⁵.

For the experiments the n-type silicon, grown by the Czochralski method with a resistivity of $0.5 \div 50 \text{ Ohm cm}$. The original silicon was doped with phosphorus (n-Si). In this case, the concentration of dopants was $7.3 \cdot 10^{13} \div 7.1 \cdot 10^{15} \text{ cm}^{-3}$ in n-Si.

The concentrations of optically active oxygen and carbon in the initial silicon samples of n- and p-type conductivity were, respectively, $N_{\text{O}}^{\text{opt}} \sim 6,2 \cdot 10^{17} \div 1,3 \cdot 10^{18} \text{ cm}^{-3}$ and carbon $N_{\text{C}}^{\text{opt}} = 2 \cdot 10^{15} \div 2 \cdot 10^{16} \text{ cm}^{-3}$. The oxygen content $N_{\text{O}}^{\text{opt}}$ and carbon $N_{\text{C}}^{\text{opt}}$ were estimated from the IR absorption spectra in the range of wave numbers $k = 1100 \text{ cm}^{-1}$ (oxygen band at $9.1 \text{ }\mu\text{m}$) and $k = 610 \text{ cm}^{-1}$ (carbon band at $16.4 \text{ }\mu\text{m}$), measured on a SpecordIR-75 infrared spectrophotometer in a two-beam scheme at 300 K ²⁶. As a control (reference) sample, we used polished oxygen-free silicon of the same thickness as the sample under study, with $N_{\text{O}}^{\text{opt}} \leq 10^{16} \text{ cm}^{-3}$, $N_{\text{C}}^{\text{opt}} = 5 \cdot 10^{15} \text{ cm}^{-3}$.

The samples were irradiated with a proton with an energy of 300 keV and a current of $1 \text{ }\mu\text{A}$. The irradiation time was different, that is, 10, 20, 30 minutes (the intensity of the beams is $10^{12} \text{ cm}^{-2}\text{s}^{-1}$).

Irradiation with protons was carried out at the unique object of the SOCOL EG-2 electrostatic accelerator at the Research Institute of Physics Semiconductors and Microelectronics.

In the Raman spectrum, the x axis is called the Raman shift and this denotes the wavelength that affects the sample. The y axis denotes the intensity of impurities in the samples. On Figure 10 the Raman spectrum of the starting silicon n-Si is shown.

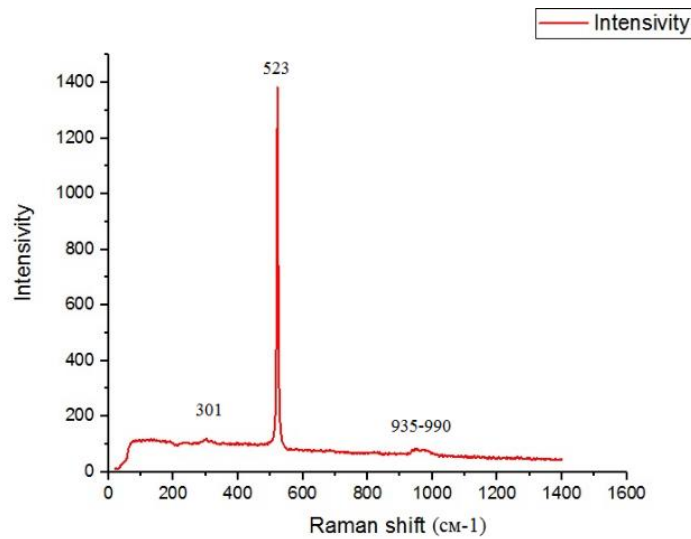
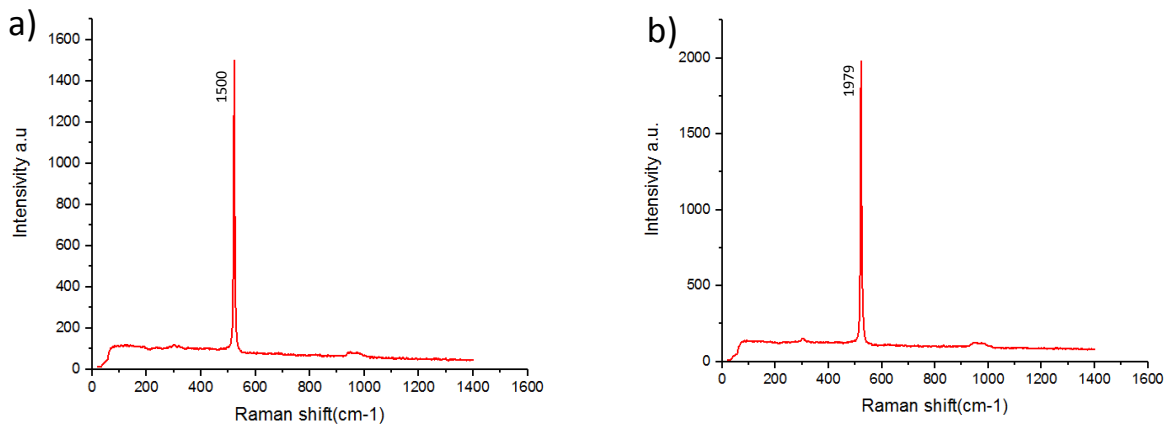


Fig.10. Raman spectrum of initial n-Si silicon.

We can see a there is one large peak (523cm^{-1}) and two small peaks ($301, 935\text{-}990\text{ cm}^{-1}$). The peaks located at $301, 523,$ and $935\text{--}990\text{ cm}^{-1}$ are introduced from the silicon substrate, which is compared with the Raman spectrum of a silicon substrate²⁷. Peak 523 cm^{-1} is the backbone of the silicon peak. Vibrations of P-O in equivalent tetrahedra $[\text{PO}_4]$ give the main Raman band at 972cm^{-1} [²⁸]. That is, these peaks denote the original silicon (doped with nothing) n-Si. In this sample, the value of the intensity of the peak 523 is equal to almost 1400 . And now we will discuss the Romanov spectra of silicon samples irradiated with 300 keV energy, $1\mu\text{A}$ current with various doses.



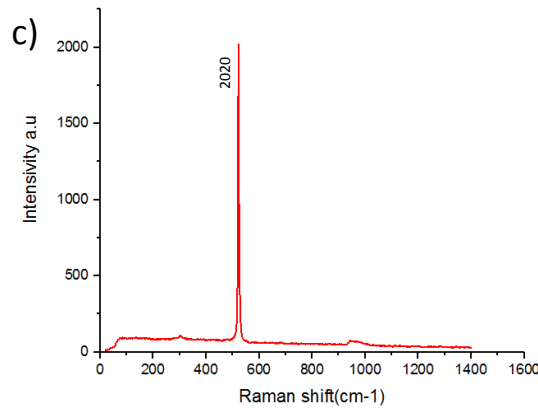


Fig.11.Raman spectrum of silicon n-Si, irradiated with protons: a) irradiated for 10 minutes; b) irradiated for 20 minutes; c) irradiated for 30 minutes (intensity of beams $10^{12} \text{ cm}^{-2}\text{s}^{-1}$).

After irradiation with protons for 10 minutes, the Raman spectrum did not change along the x axis, because the impurity composition of the sample did not change after irradiation. But the intensity of the 523 peak is increased to 1500 (Fig. 11a).

After irradiation for 20 and 30 minutes, the location of the peaks along the x axis also did not change due to the unchanged impurity composition (Fig. 11b, 11c). But, the intensity of point 523 has increased in large numbers. The intensity of the sample that was irradiated for 20 minutes is increased to 1979. The intensity of the sample that is irradiated for 30 minutes is increased to 2020. This means that the intensity of the beam is directly proportional to the dose of protons.

We know that the intensity is the average power carried by the wave through a unit area located perpendicular to the direction of wave propagation, the energy flux density, that is, the amount of energy passing per unit of time through a unit of area. We also know that power is always directly proportional to resistance. We have seen that when the dose of irradiation of the sample was increased, the intensity of the beam in Raman spectroscopy also increased. This means that the radiation dose

changes the electrical resistance of the silicon samples. How many doses you irradiate, so much the resistivity of silicon samples increases.

4. Conclusion

After irradiation with protons and alpha particles, the electrical conductivity properties of semiconductor materials drop sharply by almost 100 times. In turn, metals have high electrical conductivity, this property is 10^5 times higher than that of semiconductors. Therefore, to improve the electrical conductivity of semiconductors, it is necessary to dope them with transition elements. As a result, we get a new radiation-resistant conductive semiconductor material. It is advantageous to create devices, diodes, transistors and other types of semiconductor devices from such materials. These devices are used in places with a high dose of radiation. For example, in a nuclear power plant, in outer space, in a reactor, etc.

5. Acknowledgements

I want to thank the organizers of the START program, the International Intergovernmental Organization for giving me such an opportunity to work at JINR, and the JINR Educational and Research Center for organizing the program with good facilities. I also want to thank my supervisor Aleksandr Doroshkevich for his trust and invitation to the START program.

During the internship, I managed to study a lot and do some experiments. I would like to thank all the scientists of the group EG-5, some JINR scientists, for example O.Yu. Ivanshina (FLNP), I. G. Genov (FLNP), V.A. Kinev (Dubna University) and F.S. Napolskiy (Dubna University, Engineering Center) who helped me to do experiments.

I also want to say a big thank to Elena Karpova, Yulia Rybachuk and Olga Reshetova, employees of the JINR Educational and Scientific Center for everything that they helped me with their advice during internship.

I also want to thank my supervisor Sh.B. Utamurodova and the direction of our institute "Physics of Semiconductors and Microelectronics at NUUz" for allowing me to participate in this program and giving good advice.

6. References

1. Д.А. Ложкина, А.М. Румянцев, Е.В. Астрова. Импедансная спектроскопия пористых кремниевых и кремний-углеродных анодов, полученных спеканием. // Физика и техника полупроводников, 2020, том 54, вып. 3. С.310-318.
2. A.Sartori, M.Orlandi, S.Berardi and others. Functionalized p-silicon photocathodes for solar fuels applications: Insights from electrochemical impedance spectroscopy. 2018, Issue 4686. Pp.30714(1-15).
3. F.Paloukis, C.Elmasides and others. Electrochemical Impedance Spectroscopy study in micro-grain structured amorphous silicon anodes for lithium-ion batteries. Journal of Power Sources. 2016, Issue 331. Pp.285-292.
4. A. Bouzidi, W. Jilani, I.S. Yahia, H.Y. Zahran . Impedance spectroscopy of monocrystalline silicon solar cells for photosensor applications: Highly sensitive device. // Physica B: Physics of Condensed Matter. 2020, issue 4526. Pp.30384(1-13).
5. H.S.Magar, R.Y.Hassan, A.Mulchandani. Electrochemical Impedance Spectroscopy (EIS): Principles, Construction, and Biosensing Applications. // Sensors. 2021, issue 21, Pp.6578(1-21).
6. Е.С.Буянова, Ю.В.Емельянова. Импедансная спектроскопия электролитических материалов. // Руководство к лабораторному практикуму дисциплины. 2008, Екатеринбург, С.40.
7. Ю.В.Емельянова, М.В.Морозова, З.А.Михайловская, Е.С.Буянова. Импедансная спектроскопия: теория и применение. // Учебное пособие. 2017г, Екатеринбург, издательство Уральского университета. С.158.
8. D.Ge, Y.Zhang, H.Chen. Effect of patterned silicon nitride substrate on Raman scattering and stress of graphene. // Materials and Design. 2021, Issue 198. Pp.109338(1-7).
9. R.K.Avasarala, T.Jena, S.K.Balivada, Ch.Angani, H.Syed, V.R.Soma, G.K.Podagatlapalli. Gold-coated silicon nanoripples achieved via picosecond

- laser ablation for surface enhanced Raman scattering studies. // Results in Optics. 2021, Issue 5. Pp.100153(1-11).
- 10.O.A. Lukianova, A.A. Parkhomenko, V.V. Krasilnikov, A.N. Khmara, A.P. Kuzmenko. New method of free silicon determination in pressureless sintered silicon nitride by Raman spectroscopy and XRD. // Ceramics International. 2019, issue 8842. Pp.30973(1-7).
 - 11.M.Kadlechikova, J.Breza, L.Vanco, M.Mikolasek, M.Hubenak. Raman spectroscopy of porous silicon substrates. // Optics. 2018, issue 4026. Pp.31233(1-6).
 - 12.Y.Suzuki, T.Park, K.Hachiya, T.Goto. Raman Spectroscopy for Determination of Silicon Oxyfluoride Structure in Fluoride Melts. // Journal of Fluorine Chemistry. 2020, issue 1139, Pp.30314(1-6)
 - 13.Y.Huang, Y.Zeng, Zh.Zhang. UV-Raman scattering of thin film Si with ultrathin silicon oxide tunnel contact for high efficiency crystal silicon solar cells. // Solar Energy Materials and Solar Cells. 2019, issue 192. Pp. 154–160.
 - 14.W.Niemeic, P.Szczygiel, P.Jelen, M.Handke. IR investigation on silicon oxycarbide structure obtained from precursors with 1:1 silicon to carbon atoms ratio and various carbon atoms distribution. // Journal of molecular structure. 2018, 1164, Pp.217-226.
 - 15.A.N.Lukianov, N.I.Klyui, B.Sha and others. Nonstoichiometric amorphous silicon carbide films as promising antireflection and protective coatings for germanium in IR spectral range. // Optical materials, 88(2019). Pp.445-450.
 - 16.B.Sha, A.N.Lukianov, M.G.Dushaiko and others. Carbon-rich amorphous silicon carbide and silicon carbonitride films for silicon-based photoelectric devices and optical elements: Application from UV to mid-IR spectral range. // Optical materials, 106(2020). Pp.109959(1-10).

17. Ш.Махкамов, Р.А.Муминов и др. Формирование радиационных дефектов в кремниевых солнечных элементах, легированном цинком. // Гелиотехника. 2013, №4. С.3-9.
18. Известия НАН Армении, Физика, т.41, №2, с.140-147 (2006).
19. В.А.Козлов, В.В.Козловский. Легирование полупроводников радиационными дефектами при облучении протонами и альфа-частицами // Физика и техника полупроводников, 2001, том 35, вып. 7. С.769-795.
20. Д.А.Хонбутаева, Н.А.Козимжонов и другие. Влияние гамма-излучения на солнечный элемент. // Universum: технические науки. 2020, №10(79). С.18-22.
21. В.М.Бабич, Н.И.Блецкан, Е.Ф.Венгер. Кислород в монокристаллах кремния. // Киев, «Интерпрес ЛТД», 1997. С.241.
22. Ш.Б.Утамурадова, З.О.Олимбеков, Д.А.Рахманов. ИК-спектроскопия кремния, легированного платиной. // Материалы международной научной конференции «Тенденции развития физики конденсированных сред», часть 2, Фергана 2021. С.255-257.
23. Н.М. Богатов, Л.Р. Григорьян, А.И. Коваленко, М.С. Коваленко, Ф.А. Колоколов, Л.С. Лунин. Влияние радиационных дефектов, созданных низкоэнергетическими протонами при температуре 83 К, на характеристики кремниевых фотоэлектрических структур // Физика и техника полупроводников, 2020, том 54, вып. 2.
24. S. Z. Zainabiddinov and Kh. S. Daliev, *Defect formation in silicon* (Tashkent: University, 1993).
25. Утамурадова Ш. Б., Далиев Х. С., Далиев Ш. Х., Файзуллаев К. М. // Прикладная физика. 2019. № 6. С. 90.
26. Sh. B. Utamuradova, *Science and World* **54**, 12 (2018).
27. *Coatings* 2018, 8, 431; doi:10.3390/coatings8120431.
28. *J.Raman Spectrosc.* **2017**, 48, 1518-1527